Stabilization of miniemulsion droplets by cerium oxide nanoparticles: a step toward the elaboration of armored composite latexes

Nancy Zgheib, Jean-Luc Putaux, Antoine Thill, Franck D'agosto, Muriel Lansalot, Elodie Bourgeat-Lami

Stabilization of miniemulsion droplets by cerium oxide nanoparticles: a step towards the elaboration of armored composite latexes

Nancy Zgheib[1], Jean-Luc Putaux[2], Antoine Thill[3], Franck D'Agosto[1], Muriel Lansalot[1], Elodie Bourgeat-Lami[1*]*

[1] Université de Lyon, Univ. Lyon 1, CPE Lyon, CNRS UMR5265, Laboratoire de Chimie, Catalyse, Polymères et Procédés (C2P2), LCPP team, 43 Bd du 11 Novembre 1918, 69616 Villeurbanne, France.

[2] Centre de Recherches sur les Macromolécules Végétales (CERMAV-CNRS), BP 53, 38041 Grenoble cedex 9, France - *affiliated with Université Joseph Fourier and member of the Institut de Chimie Moléculaire de Grenoble*

[3] CEA, IRAMIS, Laboratoire Interdisciplinaire sur l'Organisation Nanométrique et Supramoléculaire, 91191 Gif-sur-Yvette, France

lansalot@lcpp.cpe.fr; bourgeat@lcpp.cpe.fr

RECEIVED DATE (to be automatically inserted after your manuscript is accepted if required according to the journal that you are submitting your paper to)

ABSTRACT

Stable methyl methacrylate (MMA) miniemulsions were successfully prepared using for the first time cerium oxide (CeO_2) nanoparticles as solid stabilizers in the absence of any molecular surfactant. The interaction between MMA droplets and CeO_2 nanoparticles was induced by the use of methacrylic acid (MAA) as a comonomer. Both MAA and CeO_2 contents played a key role on the diameter and the stability of the droplets formed during the emulsification step. Cryo-TEM images of the suspensions formed with 35 wt% of CeO_2 showed the presence of polydisperse 50-150 nm spherical droplets. More surprisingly, some non-spherical (likely discoidal) objects that could be the result of the sonication step were also observed. The subsequent polymerization of these Pickering miniemulsion droplets led to the formation of composite PMMA latex particles armored with CeO_2. In all cases, the conversion was limited to ca. 85%, concomitant with a loss of stability of the latex for CeO_2 contents lower than 35 wt%. This stability issues were likely related to the screening of the cationic charges present on CeO_2 nanoparticles upon polymerization. TEM images showed mostly spherical particles with a diameter ranging from 100 to 400 nm and homogeneously covered with CeO_2. Besides, for particles typically larger than 200 nm a buckled morphology was observed supporting the presence of residual monomer at the end of the polymerization and consistent with the limited conversion. The versatility of these systems was further demonstrated using 35 wt% of CeO_2 and replacing MMA by *n*-butyl acrylate (BA) either alone or in combination with MMA. Stable monomer emulsions were always obtained, the droplet size increasing with the hydrophobicity of the oil phase, pointing out the key influence of the wettability of the solid stabilizer. The polymerization of Pickering miniemulsion stabilized by CeO_2 nanoparticles proved to be an efficient strategy to form armored composite latex particles which may find applications in coating technology.

KEYWORDS: Pickering stabilization, cerium oxide, miniemulsion, polymerization, armored particles, cryo-TEM

Introduction

Over a century ago, Ramsden[1] and Pickering[2] observed that colloidal particles located at the oil-water interface were able to stabilize emulsions of both the oil-in-water (O/W) and the water-in-oil (W/O) type. These are referred to as either Pickering emulsions or solid-stabilized emulsions.[3] One of the key parameters to prepare stable Pickering emulsions is the wettability of the nanoparticles at the oil-water interface, which determines the type of the emulsion and can be estimated by the contact angle θ the nanoparticle makes with the interface. Indeed, hydrophilic particles ($\theta < 90°$) stabilize O/W emulsions, while hydrophobic particles ($\theta > 90°$) stabilize W/O emulsions. It is now well-established that particles, once at interfaces, can be thought of as irreversibly adsorbed due to their very high attachment energy (unlike molecular surfactants) and that the adhesion becomes stronger when the particle size increases.[4] However, the binding of small nanoparticles to liquid interfaces is much weaker (typically 1–100 kT) and the competition between the adhesion forces and Brownian motion leads to the reversibility of the adsorption,[5, 6] which has been experimentally demonstrated.[7]

In line with these concepts, the polymer community has recently shown a surge of interest for the production of a vast range of hybrid colloidal materials using various nanoparticles as solid stabilizers for emulsion[8-16] or miniemulsion polymerization.[17-25] The advantages of the "Pickering" technology for latex synthesis are twofold. First, inorganic solid stabilizers should limit the diffusion issues usually encountered with molecular surfactants in the post-applications (coatings for instance) of the hybrid particles. Secondly, the *in situ* synthesis of latexes stabilized by inorganic particles is an elegant tool to create organic/inorganic hybrid particles which can provide enhanced mechanical and physical properties for various applications.[26, 27] In particular, the armored morphologies obtained through Pickering (mini)emulsion polymerization have already shown to improve mechanical properties in adhesives[20] and coatings[14, 28, 29, 30] applications.

The concept of polymerizing Pickering miniemulsions seems particularly attractive. First, the particle formation is in theory easier than in the case of emulsion polymerization. Indeed, if the preparation of a stable miniemulsion is successful, the obtained particles should give a rather accurate image of the initial system. Besides, considering that miniemulsion droplets can be regarded as individual nanoreactors, it is relatively easy to encapsulate organophilic compounds (dyes, polymers, nanoparticles) by this technique.[31] Finally, miniemulsion polymerization offers great opportunities for conducting reactions under non-conventional conditions. Aqueous catalytic polymerization, controlled radical polymerization, polycondensation or polyaddition reactions have successfully been performed in miniemulsion droplets.[32] Regarding Pickering miniemulsions, clays (either Laponite[18-20] or Montmorillonite[24, 25]) and silica[17, 21-23, 33] have already been tested following this strategy, to fabricate either particles or capsules. The stability of the initial miniemulsion, which is a key point to ensure the formation of a stable latex, can be affected by various parameters such as the concentration of the nanoparticles, the chemical modification of their surface, the pH or the presence of salt.

Beside clays and silica, cerium dioxide (CeO_2) is also a potential candidate as a Pickering stabilizer in miniemulsion polymerization. CeO_2 nanoparticles are cationic nanocrystalline particles which have recently attracted considerable attention due to their catalytic properties, their resistance to abrasion and their unique optical features (anti-UV filter).[34-39] For instance, these nanoparticles are currently used in applications such as wood varnish,[40-43] glass polishing,[44] or catalytic converters.[45]

In this paper, we report on the use of CeO_2 nanoparticles as solid stabilizers for both starting monomer emulsions and final polymer particles. Playing with the interaction between the surface of methyl methacrylate (MMA) droplets and that of CeO_2 nanoparticles, stable MMA miniemulsions were formed via ultrasonication in the absence of any surfactant. The obtained miniemulsions were then polymerized. The influence of the MAA and CeO_2 contents on the size

of both MMA droplets and PMMA particles will be discussed, as well as the influence of the monomer nature.

Experimental Section

Materials. Water was deionized before use (Purelab Classic UV, Elga LabWater). Methyl methacrylate (MMA, 99%, Aldrich), *n*-butyl acrylate (BA, 99+%, Aldrich), styrene (S, 99%, Aldrich), methacrylic acid (MAA, 99.5%, Acros Organics), octadecyl acrylate (ODA, 97%, Aldrich), isobutyric acid (IA, 99%, Aldrich), 2,2'-azoisobutyramidine dihydrochloride (AIBA, 97%, Aldrich) and 2,2'-Azobis(isobutyronitrile) (AIBN, Fluka, 98%) were used as received. Cerium oxide nanoparticles (hereafter referred to as nanoceria) were kindly provided as an aqueous dispersion (20 wt%) by the Rare Earths team from Rhodia Recherches (Aubervilliers, France).

Miniemulsion polymerization procedures. Batch miniemulsion (co)polymerizations were performed in a glass-jacketed reactor equipped with a condenser and a nitrogen inlet. The monomers (MMA, MMA/BA or BA) were first mixed with the costabilizer (ODA) and the initiator (if monomer-soluble, i.e. AIBN). This organic phase was then added to the aqueous solution containing CeO_2 nanoparticles under vigorous stirring. After 5 min, the resulting mixture was ultrasonicated (750 W Vibracell 75042, amplitude 67%) for 5 min. Then, the obtained miniemulsion was either subjected to an in-depth characterization or introduced into the reactor to be polymerized. In this case, the mixture was deoxygenated by purging with nitrogen for 20 min while the temperature was raised to 70°C. The addition of the water-soluble initiator AIBA gave the zero time of the polymerization. Depending on the experiments, MAA was introduced either into the aqueous phase or in the monomer solution. The experimental conditions of the prepared MMA miniemulsions and of the various polymerizations performed for this study are presented in Table 1 and Table 2, respectively.

Characterization

CeO_2 nanoparticles. The CeO_2 nanoparticles were characterized by X-ray diffraction (XRD) using a Bruker® D8 Advance diffractometer, with CuKα radiation in a Bragg-Brentano geometry. High-resolution transmission electron microscopy (HRTEM) was carried out on a JEOL 2200 FS microscope operating at 200 kV. The specific surface area (S_{spec}) was determined from nitrogen adsorption isotherms using the Brunaeur, Emmett, Teller (BET) method.[46] Small-angle X-ray scattering (SAXS) data were collected on a custom experimental set-up including a rotating anode and collimating optics providing a monochromatic beam (λ = 0.1548 nm) of 2×2 mm^2 at the sample position with a total incident flux of 8.10^7 photons/s. The transmitted flux was continuously measured with a photodiode placed on the beam stop. A MAR research X-ray sensitive 300 mm plate detector was placed after the output window of the vacuum chamber at a distance of 1200 mm from the sample. A ratio q_{max}/q_{min} of 34 was reached with q_{max} = 0.5 $Å^{-1}$ and q_{min} = 0.015 $Å^{-1}$. The scattering vector q is defined as $q = k_d - k_i$ (the wave vectors of the incident and scattered beams) and has a modulus of $q = 4\pi/\lambda \sin(\theta)$ where λ is the incident wavelength and 2θ is the scattering angle. The samples were introduced in kapton cells. The counting time was 3600 s and the signal was corrected for background. Standard procedures were applied to obtain the scattered intensity in cm^{-1} as a function of scattering vector q.[47]

Miniemulsions and latexes. The droplet and particle size (hydrodynamic diameters – D_d and D_p, respectively) and the polydispersity of the sample (*Poly* - the higher this value, the broader the size distribution) were measured by dynamic light scattering (DLS) using a Zetasizer HS1000 from Malvern Instruments. The data were collected using the fully automatic mode of the Zetasizer system, and depending on the size distribution, either the monomodal analysis (the so-called cumulant analysis) or the Contin analysis was performed. The number of droplets or particles (N_d or N_p, respectively) was calculated using the diameter obtained from DLS (either D_d or D_p) according to equation (1). SC is the solid content of the dispersed phase (comprising

cerium oxide, the monomer and the polymer present for a given conversion and expressed in $g.mL^{-1}_{Latex}$), and ρ ($g.cm^{-3}$) the density of the particles (taking into account the conversion).

$$N_{d,p} = \frac{6\tau}{\rho\pi D_{d,p}^{\ 3}} \qquad (1)$$

The monomer consumption was followed by gravimetric analysis of samples taken from the polymerization medium at different times. For rapid transmission electron microscopy (TEM) examination, drops of dilute latex suspensions were deposited on formvar-coated copper grids and allowed to evaporate. The preparations were observed at room temperature with a Philips CM120 microscope operating at an accelerating voltage of 80 kV (Centre Technologique des Microstructures (CTμ), Université Claude Bernard, Villeurbanne, France). A sample of Latex 2 was isolated just before destabilization (t = 50 min, conversion = 80%, Table 2), centrifuged, dried at 110°C and embedded in an epoxy resin. Ultrathin sections (50–100 nm) were obtained at room temperature, using a Leica Ultracut E ultramicrotome equipped with a diamond knife. The ultrathin sections were deposited on TEM grids and observed without staining.

To prevent deformation/degradation of the liquid monomer droplets or the soft latex particles due to drying and/or radiation damage at room temperature, two other techniques were used. According to the method described elsewhere,[14] thin liquid films of the suspensions were formed on NetMesh lacy carbon films (Pelco International, USA) and quench-frozen in liquid ethane using a Leica EM CPC workstation (Leica Microsystems, Austria). The specimens were mounted on a precooled Gatan 626 specimen holder, transferred in the microscope and observed at low temperature (-180°C). The second technique consisted in depositing a drop of the latex suspension on a continuous carbon film, blotting the water in excess and mounting the dry specimen on the Gatan holder, at room temperature. Once transferred in the microscope, the holder was cooled down to -180°C, and the specimen was observed. This method allowed the observation of the latex particles with a high contrast since they were not embedded in a film of vitreous ice, like in the cryo-TEM protocol previously described. Both types of specimens were

observed with a Philips CM200 'Cryo' microscope operating at 80 kV, under low dose conditions. The images were recorded on Kodak SO163 films. SAXS analyses of CeO_2-stabilized MMA miniemulsion were performed using the experimental set-up described in the previous section.

Results and Discussion

CeO_2 nanoparticles. The aqueous dispersion of CeO_2 nanoparticles was synthesized by the precipitation of $Ce^{4+}(NO_3^-)_4$ salt in an acidic solution of HNO_3. The resulting $CeO_2(HNO_3)_{0.5}(H_2O)_4$ precipitate spontaneously redispersed in water to produce a colloidal sol stable at a pH ranging from 0.5 to 2.5. The surface was, however, quite heterogeneous with covalently linked hydroxyl and nitrate groups, and was surrounded by NO_3^- and H^+ counterions.[48, 49] The surface of the nanoceria was positively charged with an isoelectric point of 7. Above pH 4, the sol was unstable. As seen in the TEM image in Figure 1a, the nanoceria corresponded to clusters of ca. 2 nm faceted units. HRTEM lattice images showed that the clusters were constituted of connected particles with various orientations with respect to one another. XRD data revealed a face centered cubic structure.[50, 51] The DLS analysis indicated a hydrodynamic diameter of 7 nm (*Poly* = 0.09) in good agreement with the size of the clusters observed by TEM. SAXS data gave further insight into the structure of the nanoceria. The experimental intensity profiles shown in Figure 2 were compared to the scattered intensity of simple models composed of spherical crystallites having the ceria crystal structure calculated using the Debye approximation.[52] In the limiting case of monodisperse crystallites, the model composed of an average of 7 crystallites with an average diameter of 2.7 nm gave the best agreement. The polydispersity in both the size and the position of the crystallites explains the discrepancy between the smooth shape of the experimental curve and the oscillations predicted by the simple model. The model does not take into account the interactions between the clusters which are responsible for the low angle intensity decrease and the presence of an interaction

peak at q~0.05 $Å^{-1}$. However, the consistency between the intensity level and the average slope of the large angle part of the intensity curve indicates that the model cluster corresponds to the correct mass and surface. One CeO_2 cluster would have an apparent average diameter of 8.1 nm and an apparent density of 2.6 $g.cm^{-3}$. These values will be used in the rest of the study. In addition, the specific surface area determined by BET was 219 $m^2.g^{-1}$.

Preparation of CeO_2-stabilized miniemulsions. In the first part of this work, CeO_2 nanoparticles were investigated as solid stabilizers for MMA droplets formed via ultrasonication in the absence of any surfactant. Considering the affinity of CeO_2 for carboxylic acids,[41, 42, 53] the wettability of the nanoparticles was adjusted by the addition of methacrylic acid (MAA) to render CeO_2 partially hydrophobic. The use of a comonomer to induce the interaction between monomer droplets and inorganic stabilizers during the preparation of a miniemulsion has previously been reported for silica nanoparticles.[17, 22, 33] MAA was chosen for both its solubility in MMA and its ability to be copolymerized with MMA, in order to strengthen the attachment of CeO_2 to the surface of the polymer particles. The interaction between MAA and CeO_2 being strong, MAA was introduced in the monomer phase to prevent any destabilization of the nanoparticles before the homogenization step. Nevertheless, MAA is also highly water-soluble and can easily diffuse to the aqueous phase and interact with the nanoceria. ODA was used to prevent Ostwald ripening. The effectiveness of the CeO_2 nanoparticles in stabilizing such miniemulsions was investigated by studying the effect of the initial concentrations of CeO_2 and MAA on the average droplet size and the miniemulsion stability. A preliminary study (25 wt% of CeO_2/MMA and 1.85 µmol of MAA per square meter of CeO_2 surface, noted as 1.85 $µmol.m^{-2}$ of MAA, data not shown) indicated that 5 min of sonication was enough to reach a stable MMA miniemulsion and that the droplet size (around 135 nm) was the same if MAA was initially introduced in the aqueous phase.

Influence of methacrylic acid concentration on the monomer droplet size

In this series of experiments, MMA miniemulsions were prepared with various MAA concentrations ranging from 0 to 7 µmol.m^{-2} keeping constant the CeO_2 content (25 wt%/MMA). When MAA was absent, no miniemulsion could be formed. Whatever the initial amount of CeO_2, the obtained MMA miniemulsions were stable (Table 1). This first observation demonstrates the Pickering stabilizer behavior of MAA-complexed CeO_2 nanoparticles. The droplet diameter, D_d, decreased with an increasing amount of MAA to reach a minimum value for 1.85 µmol.m^{-2} before steadily increasing again (Figure 3). The size distribution (indicated by the *Poly* value from the Zetasizer) followed the same trend. Due to its high water solubility, MAA likely interacted with CeO_2 nanoparticles in the water phase and made the CeO_2 particles more hydrophobic, which promoted its adhesion at the MMA/water interface. For MAA concentrations lower than 1.85 µmol.m^{-2}, the decrease in monomer droplet size and size distribution as the MAA concentration increases could mainly be attributed to a higher number of CeO_2 nanoparticles located at the MMA/water interface allowing a higher surface area to be covered. This was clearly favored by an increasing number of carboxylic acid functions that improved the interaction of CeO_2 with the monomer phase. The steady increase of D_d and *Poly* when the MAA concentration was higher than 1.85 µmol.m^{-2} came from a less efficient coverage of the MMA droplets by the nanoparticles. Indeed, when the MAA concentration was such that the CeO_2 nanoparticles were fully covered, the nanoparticles rapidly aggregated before their adsorption on MMA droplets, resulting in a less efficient stabilization of the miniemulsion. Figure 3 shows that the optimal amount of MAA needed to form the smallest droplets with a low size distribution is close to 1.85 µmol.m^{-2}. It is worth mentioning that the SAXS analysis of an aqueous dispersion of CeO_2 formed in the presence of 1.85 µmol.m^{-2} of MAA confirmed that the addition of MAA at this concentration had no impact on the size of the CeO_2 clusters which could account for the efficient stabilization of the monomer droplets in this case (See Supporting Information Figure S1).

Influence of CeO_2 content on MMA droplet size

Various amounts of CeO_2 have been tested to determine the minimal amount of nanoparticles required to form a stable MMA miniemulsion. In each case, the surface coverage, *Cov*, defined as the fraction of the droplet surface, a_d, actually covered by the CeO_2 particles, was calculated. We assumed that (i) CeO_2 was composed of 8.1 nm-large spherical clusters as previously determined by SAXS; (ii) all CeO_2 nanoparticles were present at the surface of the monomer droplets; (iii) CeO_2 and MMA droplets were uniform in size; (iv) the size of CeO_2 particles was negligible with respect to the size of MMA droplets (curvature and geometrical constraints were neglected). Finally, we assumed that (v) the surface area occupied by one CeO_2 cluster at the droplet surface was equal to the cross-sectional area of a plane bisecting that cluster. Taking into account all these assumptions, the surface coverage can then be expressed as:

$$Cov\,(\%) = \frac{1}{4}\left(\frac{m_{CeO_2}}{m_M}\right)\left(\frac{\rho_m}{\rho_{CeO_2}}\right)\left(\frac{D_d}{D_{CeO_2}}\right)\times 100 \quad (2)$$

where m_{CeO_2} is the amount of CeO_2 clusters, ρ_{CeO_2} their apparent density and D_{CeO_2} their diameter, m_M the combined amount of monomers (MMA and MAA) and costabilizer (ODA), ρ_M the combined density of monomers (MMA and MAA) and costabilizer (ODA) and D_d the droplet diameter (see the Supporting Information for the detailed calculations).

The intensity average DLS diameter, the size distribution (i.e. *Poly* values) and the surface coverage of MMA droplets for various initial CeO_2 amounts are given in Table 1. When the CeO_2 content increases, the droplet diameter decreases (without noticeable impact on the *Poly* values) and the surface coverage increases. Thus, a minimal amount of CeO_2 must be introduced to obtain a high surface coverage and to form small size droplets. According to the surface coverage values reported in Table 1, the full coverage of MMA droplet has never been reached,

even for high CeO_2 content (35 wt%/MMA). These data would indicate that CeO_2 clusters do not form a dense layer at the surface of the MMA droplets. This may be ascribed to the electrostatic repulsion existing between the positively charged clusters preventing a dense coverage of the droplet surface area, and possibly also to the difficulty to form a continuous layer with particles with irregular shapes. Surface coverages as low as 29% have previously been reported by Midmore[54] who formed very stable emulsions using silica nanoparticles flocculated by hydroxypropyl cellulose. This low surface coverage was explained by the possible formation of a two-dimensional gel at the O/W interface. It seems unlikely that this kind of arrangement operates in our system, but the strong charge density of the CeO_2 nanoparticles may be sufficient to lead to stable miniemulsions, even for low CeO_2 content.

Morphology and structure of CeO_2-stabilized MMA droplets

Optical microscopy is generally used to directly visualize micrometric droplets. [55] However, examples of direct observation of submicronic droplets using as stabilizers either molecules or particles are scarce. Although TEM is more suitable to characterize the size and shape of nanoparticles, problems arise for soft deformable nano-objects such as monomer droplets. A few methods have been reported in the literature to fix the morphology of styrene miniemulsions prior to TEM observation such as chemical staining and hardening with osmium tetroxide,[56] or freeze-fracture followed by replication.[57, 58]. Wet-scanning transmission electron microscopy (wet-STEM) on dilute styrene miniemulsion has also been reported.[59] However, these techniques are time-consuming and may also alter the sample integrity.

Here, we report for the first time the direct TEM and cryo-TEM observations of Pickering miniemulsion droplets stabilized by 35 wt% CeO_2 (ME8 sample in Table 1). Conventional TEM images of dried preparations show crumpled objects (Figure 5a). As the monomer evaporated

during drying, the objects likely correspond to the nanoceria envelopes that stabilized individual monomer droplets in suspension.

Cryo-TEM images of the suspension that was quench-frozen immediately after sonication are shown in Figures 5b and 5c. Polydisperse 50-150 nm spheroidal droplets can be seen, the dark outline at their periphery revealing the stabilizing layer of nanoceria. Free-standing CeO_2 clusters are also observed homogeneously distributed in the embedding ice. Variations of the average grey level on each droplet may have several origins: i) the liquid droplets were more or less flattened due to the capillary forces of the thin liquid film surfaces prior to quench-freezing; ii) the monomer was partially degraded by radiation damage during image recording and the contrast decreased; iii) the surface coverage by nanoceria clusters varied for each particle. Indeed, droplets with a very faint contrast can be detected in Figure 5b, that may correspond to monomer droplet with no – or a very small amount of – CeO_2 clusters on their surface. The presence of free nanoceria in the embedding film indicates that, for such a high CeO_2 content, not all clusters were adsorbed on monomer droplets. However, as such small nanoparticles will rapidly concentrate near the surfaces of the liquid film prior to quench-freezing, their apparent concentration is probably significantly overestimated and should thus be considered with care. Cryo-TEM observations were also performed on the suspension after one week of ageing but no significant difference could be observed in terms of shape, size or free clusters (Figure 5d). Some particles exhibited a slightly crumpled aspect and the nanoceria envelope sometimes appeared to be damaged but this could result from instabilities introduced by shearing forces during sample preparation, in particular during blotting prior to quench-freezing. These droplets may also be the result of some monomer leak leading to the shrinkage of the droplet. At some point, the rigidified shell of the droplet would start to collapse and inward buckling would ensue giving rise to the observed crumpled morphologies. Similar morphologies have been reported in the literature in the case of O/W Pickering emulsions when small amount of the oil was pumped out

of the droplet interior using either PS[60] or silica[61] particles as stabilizers, or during the dissolution of particle-covered bubbles.[62, 63]

More surprisingly, some non-spherical droplets were observed, in particular, "rectangular" particles (Figures 5c and 5d). As the image is only a projection of the particle volume, the three-dimensional shape may be parallelepipedal or, more likely, discoidal, with the disk axis lying perpendicular to the observation direction. These distorted droplets may result from the emulsification process, which requires a high input of energy. As a result, the adhesion of the clusters to the monomer/oil interface may be reversible, allowing for the formation of submicrometer size droplets. This reversibility of the adhesion has already been put forward for the successful preparation of styrene miniemulsion using Laponite clay disks as solid stabilizers.[19] However, for small particles (≤ 30 nm), studies have also reported a stronger adhesion if the particles are partially flocculated, which has been attributed to the larger size of the flocs than that of the individual particles.[54, 64-66] Besides, the addition of MAA likely increases the hydrophobicity of the particles and hence their wettability. This change in the wettability of the flocs is also in favor of a stronger adhesion.[67] Taking both the shape (aggregated state) and the wettability of the CeO_2 clusters into consideration, the observed distorted droplets may thereby be the result of the objects formed during the sonication step, frozen in these particular morphologies when the sonication stops.

These TEM observations show that the droplet diameter determined by DLS, and consequently the surface coverage, must be considered with care, since the presence of free CeO_2 may lead to overestimated surface coverages.

SAXS measurements gave additional insights into the aggregation state of the CeO_2 nanoparticles in the miniemulsion (see Supporting Information Figure S1). The oscillation of the scattered intensity at $q = 0.1$ Å^{-1} is a signature of the presence of the CeO_2 clusters. Thus, they are still present after the mixture with MMA and after the miniemulsion formation. The scattering curve also reveals that they are slightly aggregated in the miniemulsion. Indeed, the

increase of the low angle scattering intensity slope compared to the CeO_2/MAA sol indicates that the clusters are now in close contact in a relatively open structure.

Stability with time and temperature of CeO_2-stabilized MMA droplets

The shelf stability of the miniemulsion was evaluated for the ME6 sample. The droplet diameter was almost the same after 24 h at room temperature (D_{d_0} = 133 nm; $D_{d_{24h}}$ = 129 nm) and neither creaming nor sedimentation was observed. In addition, the droplet size was barely impacted when the temperature was set to 70°C ($D_{d_{RT}}$ = 133 nm; $D_{d_{70°C}}$ = 135 nm). However, at this temperature, the droplet diameter steadily increased with time ($D_{d_{70°C-6h}}$ = 163 nm). The very good stability of this kind of CeO_2-stabilized miniemulsion in regards with both time and temperature may be attributed to the Pickering stabilization mechanism. Indeed, solid stabilizers (in addition to the hydrophobic ODA component) have already been reported to slow down Ostwald ripening effects when hexadecane was added to toluene for toluene-in-water emulsions stabilized by Laponite.[66]

Polymerization of CeO_2-stabilized miniemulsions.

Influence of CeO_2 content. As shown in the previous section, stable MMA miniemulsions could be prepared in the presence of nanoceria as sole stabilizer. The CeO_2 content plays a key role on the diameter of the droplets formed during the emulsification step. With the aim of forming latex particles without molecular surfactant, the next step of our study consisted in polymerizing these MMA droplets formed in the presence of 20 to 35 wt% CeO_2 and AIBA as an initiator. Figure 6 shows the evolution of conversion with time and of particle diameter with conversion, for this series of experiments. There is no significant influence of the initial amount of CeO_2 on the kinetics. In all cases, the conversion was always limited to ca. 85% (Figure 6a).

A second addition of AIBA at t = 50 min did not result in a full conversion either. Gas chromatography analyses of these latexes showed the presence of residual MMA and thus the incomplete conversion. One may ask if the presence of CeO_2 nanoparticles could interfere with the radical polymerization. Indeed, it has previously been reported that the presence of an armoring layer of inorganic nanoparticles on the surface of polymer particles could affect the entry and exit events of the radicals in both emulsion[68] and miniemulsion polymerization.[19] In our case, the oligoradicals formed in the aqueous phase at the beginning of the polymerization can easily enter the monomer droplets if one assumes that the CeO_2 nanoparticles are initially homogeneously but not too densely distributed onto MMA droplets. However, as the polymerization proceeds, the polymer chains formed at the surface or in the vicinity of the CeO_2 clusters via the presence of MAA screen their cationic charges. In addition, the composition of the organic phase changes upon polymerization and the affinity between the particle surface and CeO_2 may also be altered due to the formation of the polymer chains. This modification of the interface nature obviously results in variations of the interfacial tension and adhesion energy of the clusters, which can influence the stability of the dispersion. If the PMMA/water interfacial tension is higher than the MMA/water one, the particles will coalesce to decrease the interfacial surface area and form bigger particles. This process would stop as soon as the O/W interface is sufficiently covered.

Both the charge screening and the alteration of the interfacial tension result in a lower capability for the CeO_2 clusters to stabilize PMMA particles compared to MMA droplets. This was experimentally illustrated by the initial increase of the particle size for conversion lower than 10% (corresponding to reaction times of 10 min) (Figure 6b and Figure S2) with a concomitant decrease in particle number (Figure 6c) indicating partial coalescence, and leading to the increase of the surface coverage (Figure 6d). These effects became even more important when the initial amount of CeO_2 decreased.

All the events described above likely lead to a closer contact between the CeO_2 nanoparticles. The interface would become more rigid and the entry of the oligoradicals would consequently be slowed down. In addition, the presence of ODA (to limit the Ostwald ripening) can strongly reduce the diffusion of the monomer out of the swollen particles and consequently limit the formation of these oligoradicals in the aqueous phase. Both phenomena (prevented radical entry and monomer diffusion) could explain the observed limitation in the conversion. It is worth noting here that the use of 2,2'-azobis(isobutyronitrile) (AIBN) in a Latex 2-type recipe (25 wt% CeO_2 and 1.85 $\mu mol.m^{-2}$) did not lift the observed limitation for the monomer conversion. After 4 h, only 60 % conversion was reached, and a plateau was still observed (data not shown).

Except for Latex 4 (35 wt% CeO_2), the plateau in conversion coincided with the loss of stability of the latexes as illustrated by the strong increase of the particle diameter (Figure 6b and Figure S2). This could be correlated with the screening of the cationic charges of the clusters as the polymerization proceeds. This screening would be such that it eventually induces the destabilization of the latex. When the CeO_2 content is high enough (*i.e.*, 35 wt%), the stability of the latex could come from free CeO_2 clusters in water, creating in the continuous phase like a 3D-network improving the stability by preventing particle-particle contact as already mentioned in the literature.[69] The evolution of the surface coverage with conversion well illustrates all the aspects discussed above in the text (Figure 6d), *i.e.*, the partial coalescence at low conversion and the loss of stability at high conversion. Whatever the mechanisms leading to the partial coalescence and to the destabilization of the latex, these systems (including the one using 35 wt% CeO_2) do not follow the expected trend of a miniemulsion polymerization (*i.e.*, nucleation of all initial droplets without any significant change in their number, and no significant migration of species) since the ratio N_p/N_d drastically decreases at the beginning of the polymerization (see Supporting Information Figure S3).

Role of MAA

When MAA was replaced by its non-polymerizable homologue, isobutyric acid (IA) (35 wt% CeO_2, 1.4 µmol.m^{-2} of MAA (Latex 5) or IA (Latex 6), Table 2), the polymerization rate was higher. A plateau value for the conversion (ca. 90%) with a strong destabilization of the latex at the end of the polymerization were observed, even with the high amount of CeO_2 used in this case (data not shown). This result clearly shows the crucial role of the presence of the covalent link between the polymer particle and the CeO_2 nanoparticles.

As the use of MAA clearly impacts the stability of the final latex, the concentration of MAA was then investigated for a Latex-2 type recipe (25 wt% CeO_2). Varying the concentration between 1.5 and 2.8 µmol.m^{-2} had no significant impact on the kinetics, with still the conversion reaching a limit at 90% (Latexes 7, 2 and 8, Table 2 and Supporting Information Figures S4 and S5). Whatever the initial MAA concentration, the latex was not stable at the end of the polymerization. However, the extent of the destabilization was less important when MAA concentration was lower. The size of the particles before destabilization was slightly higher for the highest MAA concentration (ca. 230 nm for 2.8 µmol.m^{-2} versus ca. 200 nm for 1.5 and 1.8 µmol.m^{-2}). As previously mentioned, the concentration of MAA strongly impacts the stability of CeO_2 clusters. Indeed, even if the droplet size is almost the same for the three concentrations (consistent with the obtained similar kinetic profiles), the aggregation state of CeO_2 is not the same. Indeed, whereas barely aggregated clusters are observed for MAA amounts equal or lower than 1.85 µmol.m^{-2} (D_h is close to 7 nm, SAXS does not show a significant aggregation (see Supporting Information Figure S1), aggregates of clusters are present at 2.8 µmol.m^{-2} (D_h = 34 nm). Once the polymerization begins, these aggregates are less efficient in the stabilization of the particles as illustrated by the higher particle diameter reached after the initial partial coalescence (> 200 nm) compared to the values obtained with lower MAA amounts (Figure S5).

Morphology and structure of CeO_2-stabilized PMMA particles

Figure 7 shows TEM images of the particles in a PMMA latex stabilized by 35 wt% (Latex 4, Figure 7a-c) or 25 wt% (Latex 2, Figure 7d) CeO_2. A previous observation of a dry preparation of particles at room temperature revealed that PMMA got soft under electron radiation resulting in significant deformation of the particles due to the local increase in temperature (not shown). Consequently, the latexes were observed at low temperature, either after quench-freezing of the suspensions (Figure 7a,b) or after air drying and subsequent freezing (Figure 7c). All images showed a polydisperse distribution of mostly spherical particles, with a diameter ranging from 100 to 400 nm. All particles are homogeneously covered with CeO_2 nanoparticles but the surface coverage seems to vary depending on the particle diameter. The smallest particles are not fully covered and the CeO_2 nanoclusters are visible slightly protruding out of the surface (Figure 7c). The contrast at the particle periphery tends to get darker with increasing diameter, suggesting that the surface coverage is also higher. The polydispersity in size of the latexes as well as the fact that their surface coverage seems to increase with the particle size may be related to the coalescence events described above (Figure 6b). When the particles are typically larger than 200 nm, their shapes get less regular and the biggest particles clearly exhibit a buckled morphology. This indicates that these particles likely contained unreacted monomer before TEM observation, and supports the presence of residual monomer at the end of the polymerization consistent with the limited conversion (Figure 6a).

The observed coalescence at the beginning of the polymerization (Figure 6b) and even more the loss of stability at the end make one wonder whether CeO_2 nanoparticles are located on the surface of the polymer particles or rather distributed inside. To check this point, a latex sample was isolated just before the destabilization (Latex 2, t = 50 min, conversion = 80%) and embedded after drying in an epoxy resin. A typical TEM image of an ultrathin section of this sample is shown in Figure 7d. The general features in terms of size and shape are very similar to

that observed in the cryo-TEM images of Latex 4 (Figures 7a and 7b). The largest particles are also buckled. The variation in the thickness of the nanoceria envelope has to be considered with care as it mostly depends on the position of the sectioning with respect to each particle. A dark and thin outline means that the particles have been cut through their center whereas a thick peripheral layer suggests that the section was more tangential. As the central regions, corresponding to the polymer, are uniformly white, we can conclude that no CeO_2 is present inside the particles (Figure 7d). These observations indicate that the destabilization of the particles at the end of the polymerization is not related to the entrapment of CeO_2 nanoparticles but related to the lack of stability of the particles at the beginning of the polymerization when coalescence is observed.

Influence of the monomer nature

In the previous experiments, MMA was used to demonstrate that CeO_2 was able to play the role of a solid stabilizer in Pickering miniemulsion polymerizations. However, the latexes used in coating applications exhibit lower glass transition temperature T_g (close to the ambient) than that of PMMA-based latexes (*i.e.*, close to 100°C). With that in mind, we performed a set of experiments using either *n*-butyl acrylate (BA, Latex 9) instead of MMA (Latex 5) or a mixture of MMA and BA (50/50 wt%, Latex 10). In the latter case, the obtained latex was expected to show a T_g close to 5°C. For this series of experiments, the amount of CeO_2 was kept to 35 wt% using 1.4 $\mu mol.m^{-2}$ of MAA, (Table 3), concentration for which the stability of the miniemulsion was still ensured whatever the monomer(s) used. This shows the versatile use of CeO_2 as Pickering stabilizer for droplets of various hydrophobic monomers but the droplet size changed with the nature of the monomer (Table 2). Indeed, the droplet size increased with the hydrophobicity of the oil phase, pointing out again the key influence of the wettability of the solid stabilizer. In all cases, the obtained latexes showed no sign of destabilization. The final conversion was higher for the MMA/BA mixture (96%) than for MMA (86%) or BA (92%)

(Figure 8). The polymerization was, however, slightly slower when BA was used, alone or in combination. These preliminary experiments suggest that the hydrophobic/hydrophilic nature of the monomer or of the mixture of monomers is an important parameter that will not only affect the rate of polymerization as it is typically observed in miniemulsion polymerization, but also the stabilizing capability of the CeO_2 clusters. This is clearly illustrated in Figure 9. Cryo-TEM images of the pure PBA sample show CeO_2-stabilized PBA particles together with some spherical "assemblies" of CeO_2 nanoclusters with an ill-defined interface but remindful of the CeO_2-armored particles (Figure 9a). On some particles, the CeO_2 armoring layer appears to have been destabilized, perhaps due to shearing forces during sample preparation, and starts to detach from the PBA particle surface (Figure 9b). Even if stable latexes were obtained with both PMAA and PBA, the interaction between CeO_2 and the PBA particles is clearly different from what was observed with PMMA.

Conclusion

Stable monomer miniemulsions were successfully prepared using for the first time CeO_2 as solid stabilizers in the absence of any molecular surfactant. The use of MAA as a comonomer proved to be crucial to induce the interaction between the monomer droplets of MMA and the CeO_2 nanoparticles. Both MAA and CeO_2 contents played a key role on the diameter and the stability of the droplets formed during the emulsification step. The formation of stable composite latex particles armored with CeO_2 was next investigated by polymerizing the Pickering-stabilized MMA miniemulsions using different CeO_2 amount ranging from 20 to 35 wt% and AIBA as an initiator. In all cases, partial coalescence at low conversion (< 10%) was observed. In addition, the conversion was always limited to ca. 85%, concomitant with a loss of stability of the latex for CeO_2 contents lower than 35 wt%. This stability issues were likely related to the screening of the cationic charges present on CeO_2 nanoparticles upon polymerization. Using the

highest amount of CeO_2 (35 wt%), the influence of the monomer nature was finally investigated using BA, either alone or in combination with MMA. Stable monomer emulsions were always obtained, showing the versatile use of CeO_2 as Pickering stabilizer for droplets of various hydrophobic monomers. Nevertheless, the droplet size increased with the hydrophobicity of the oil phase, pointing out the key influence of the wettability of the solid stabilizer. In all cases, the obtained latexes showed no sign of destabilization suggesting that the hydrophobic/hydrophilic nature of the monomer(s) is an important parameter affecting the stabilizing capability of CeO_2. In conclusion, the polymerization of Pickering miniemulsion stabilized by CeO_2 nanoparticles proved to be an efficient strategy to form armored composite latex particles which may find applications in coating technology.

Acknowledgments: The authors would like to thank Dr Jérôme Majimel (CNRS, Université de Bordeaux, ICMCB, Pessac, France) for the HRTEM images of nanoceria. NZ acknowledged the French Ministry for Research for financial support.

Supporting Information Available. Determination of the surface coverage. SAXS curves of MAA-modified CeO_2 and CeO_2-stabilized MMA miniemulsion. Evolution of particle diameter and of N_p/N_d versus conversion for MMA miniemulsion polymerization using various initial amounts of CeO_2 (wt%/MMA). Evolution of conversion versus time and of particle diameter versus conversion for MMA miniemulsion polymerization using various initial amounts of MAA. This information is available free of charge via the Internet at http://pubs.acs.org.

References

1. Ramsden, W. Separation of solids in the surface-layers of solutions and 'suspensions' (observations on surface-membranes, bubbles, emulsions, and mechanical coagulation). - Preliminary account. *Proc. Roy. Soc. London* **1903,** *72*, 156-164.

2. Pickering, S. U. Emulsions. *J. Chem. Soc., Trans.* **1907,** *91*, 2001-2021.

3. Binks, B. P.; Horozov, T. S., *Colloidal Particles at Liquid Interfaces*. Cambridge Univ. Press: Cambridge, 2006.

4. Binks, B. P. Particles as surfactants-similarities and differences. *Curr. Opin. Colloid Interface Sci.* **2002,** *7*, 21-41.

5. Bresme, F.; Oettel, M. Nanoparticles at fluid interfaces. *J. Phys.: Condens. Matter* **2007,** *19*, 413101.

6. Cheung, D. L.; Bon, S. A. F. Interaction of Nanoparticles with Ideal Liquid-Liquid Interfaces. *Phys. Rev. Lett.* **2009,** *102*, 066103.

7. Lin, Y.; Skaff, H.; Emrick, T.; Dinsmore, A. D.; Russell, T. P. Nanoparticle Assembly and Transport at Liquid-Liquid Interfaces. *Science* **2003,** *299*, 226-229.

8. Sacanna, S.; Kegel, W. K.; Philipse, A. P. Thermodynamically Stable Pickering Emulsions. *Phys. Rev. Lett.* **2007,** *98*, 158301-4.

9. Colver, P. J.; Colard, C. A. L.; Bon, S. A. F. Multilayered Nanocomposite Polymer Colloids Using Emulsion Polymerization Stabilized by Solid Particles. *J. Am. Chem. Soc.* **2008,** *130*, 16850-16851.

10. Schmid, A.; Tonnar, J.; Armes, S. P. A New Highly Efficient Route to Polymer-Silica Colloidal Nanocomposite Particles. *Adv. Mater.* **2008,** *20*, 3331-3336.

11. Walther, A.; Hoffmann, M.; Müller, A. H. E. Emulsion Polymerization Using Janus Particles as Stabilizers. *Angew. Chem. Int. Ed.* **2008,** *47*, 711-714.

12. Zhang, J.; Chen, K.; Zhao, H. PMMA colloid particles armored by clay layers with PDMAEMA polymer brushes. *J. Polym. Sci., Part A: Polym. Chem.* **2008,** *46*, 2632-2639.

13. Yuan, Q.; Yang, L.; Wang, M.; Wang, H.; Ge, X.; Ge, X. The Mechanism of the Formation of Multihollow Polymer Spheres through Sulfonated Polystyrene Particles. *Langmuir* **2009,** *25*, 2729-2735.

14. Bourgeat-Lami, E.; Guimarães, T. R.; Pereira, A. M. C.; Alves, G. M.; Moreira, J. C.; Putaux, J.-L.; dos Santos, A. M. High Solids Content, Soap-Free, Film-Forming Latexes Stabilized by Laponite Clay Platelets. *Macromol. Rapid Commun.* **2010,** *31*, 1874-1880.

15. Teixeira, R. F. A.; McKenzie, H. S.; Boyd, A. A.; Bon, S. A. F. Pickering Emulsion Polymerization Using Laponite Clay as Stabilizer To Prepare Armored "Soft" Polymer Latexes. *Macromolecules* **2011,** *44*, 7415-7422.

16. Fielding, L. A.; Tonnar, J.; Armes, S. P. All-Acrylic Film-Forming Colloidal Polymer/Silica Nanocomposite Particles Prepared by Aqueous Emulsion Polymerization. *Langmuir* **2011,** *27*, 11129–11144.

17. Tiarks, F.; Landfester, K.; Antonietti, M. Silica Nanoparticles as Surfactants and Fillers for Latexes Made by Miniemulsion Polymerization. *Langmuir* **2001,** *17*, 5775-5780.

18. Cauvin, S.; Colver, P. J.; Bon, S. A. F. Pickering Stabilized Miniemulsion Polymerization: Preparation of Clay Armored Latexes. *Macromolecules* **2005,** *38*, 7887-7889.

19. Bon, S. A. F.; Colver, P. J. Pickering Miniemulsion Polymerization Using Laponite Clay as a Stabilizer. *Langmuir* **2007,** *23*, 8316-8322.

20. Wang, T.; Colver, P. J.; Bon, S. A. F.; Keddie, J. L. Soft polymer and nano-clay supracolloidal particles in adhesives: synergistic effects on mechanical properties. *Soft Matter* **2009,** *5*, 3842-3849.

21. Fortuna, S.; Colard, C. A. L.; Troisi, A.; Bon, S. A. F. Packing Patterns of Silica Nanoparticles on Surfaces of Armored Polystyrene Latex Particles. *Langmuir* **2009,** *25*, 12399–12403.

22. Zhang, K.; Wu, W.; Guo, K.; Chen, J. F.; Zhang, P. Y. Magnetic polymer enhanced hybrid capsules prepared from a novel Pickering emulsion polymerization and their application in controlled drug release. *Coll. Surf. A: Phys. Eng. Asp.* **2009,** *349*, 110-116.

23. Cao, Z.; Schrade, A.; Landfester, K.; Ziener, U. Synthesis of raspberry-like organic–inorganic hybrid nanocapsules via Pickering miniemulsion polymerization: Colloidal stability and morphology. *J. Polym. Sci., Part A: Polym. Chem.* **2011,** *49*, 2382-2394.

24. Voorn, D. J.; Ming, W.; van Herk, A. M. Polymer-Clay Nanocomposite Latex Particles by Inverse Pickering Emulsion Polymerization Stabilized with Hydrophobic Montmorillonite Platelets. *Macromolecules* **2006,** *39*, 2137-2143.

25. Guillot, S.; Bergaya, F.; de Azevedo, C.; Warmont, F.; Tranchant, J.-F. Internally structured Pickering emulsions stabilized by clay mineral particles. *J. Colloid Interface Sci.* **2009,** *333*, 563-569.

26. Bourgeat-Lami, E.; Lansalot, M., Organic/Inorganic Composite Latexes: The Marriage of Emulsion Polymerization and Inorganic Chemistry. In *Hybrid Latex Particles*, van Herk, A. M.; Landfester, K., Eds. Springer Berlin / Heidelberg: 2010; Vol. 233, pp 53-123.

27. Xue, Z.; Wiese, H. Production of aqueous dispersions of particles composed of polymers and ultrafine inorganic solids. WO2003000760A1, 2003.

28. Amalvy, J. I.; Percy, M. J.; Armes, S. P.; Wiese, H. Synthesis and Characterization of Novel Film-Forming Vinyl Polymer/Silica Colloidal Nanocomposites. *Langmuir* **2001,** *17*, 4770-4778.

29. Negrete-Herrera, N.; Putaux, J.-L.; David, L.; Haas, F. D.; Bourgeat-Lami, E. Polymer/Laponite Composite Latexes: Particle Morphology, Film Microstructure, and Properties. *Macromol. Rapid Commun.* **2007,** *28*, 1567-1573.

30. Schmid, A.; Scherl, P.; Armes, S. P.; Leite, C. A. P.; Galembeck, F. Synthesis and Characterization of Film-Forming Colloidal Nanocomposite Particles Prepared via Surfactant-Free Aqueous Emulsion Copolymerization. *Macromolecules* **2009,** *42*, 3721-3728.

31. Weiss, C.; Landfester, K., Miniemulsion Polymerization as a Means to Encapsulate Organic and Inorganic Materials. In *Hybrid Latex Particles*, van Herk, A. M.; Landfester, K., Eds. Springer Berlin / Heidelberg: 2010; Vol. 233, pp 185-236.

32. Crespy, D.; Landfester, K. Miniemulsion polymerization as a versatile tool for the synthesis of functionalized polymers. *Beilstein J. Org. Chem.* **2010,** *6*, 1132-1148.

33. Schrade, A.; Mikhalevich, V.; Landfester, K.; Ziener, U. Synthesis and characterization of positively charged, alumina-coated silica/polystyrene hybrid nanoparticles via Pickering miniemulsion polymerization. *J. Polym. Sci., Part A: Polym. Chem.* **2011,** *49*, 4735-4746.

34. Flytzani-Stephanopoulos, M.; Zhu, T.; Li, Y. Ceria-based catalysts for the recovery of elemental sulfur from SO_2-laden gas streams. *Catal. Today* **2000,** *62*, 145-158.

35. Patsalas, P.; Logothetidis, S.; Metaxa, C. Optical performance of nanocrystalline transparent ceria films. *Appl. Phys. Lett.* **2002,** *81*, 466-468.

36. Robinson, R. D.; Spanier, J. E.; Zhang, F.; Chan, S. W.; Herman, I. P. Visible thermal emission from sub-band-gap laser excited cerium dioxide particles. *J. Appl. Phys.* **2002,** *92*, 1936-1941.

37. Fauchadour, D.; Jeanson, T.; Bousseau, J.-N.; Echalier, B. Nanoparticles of Cerium Oxide — Application to Coatings Technologies. *Proceedings of the 1st Nano and Hybrid Coatings Conference, Paint Research Association* **2005**, Paper 19.

38. Ouzaouit, K. PhD Dissertation, Université du Sud Toulon Var, Toulon, 2007.

39. Truffault, L. PhD Dissertation, Université d'Orléans, 2010.

40. Pattamasattayasonthi, N.; Chaochanchaikul, K.; Rosarpitak, V.; Sombatsompop, N. Effects of UV weathering and a CeO_2-based coating layer on the mechanical and structural changes of wood/PVC composites. *J. Vinyl Addit. Technol.* **2011,** *17*, 9-16.

41. Bousseau, J.-N.; Fauchadour, D.; Tolla, B. Compositions based on aqueous paints, particularly lacquers or varnishes, and aqueous colloidal dispersions of cerium. WO2003099942A1, 2003.

42. Berret, J.-F.; Morvan, M.; Sehgal, A. Aqueous transparent or semitransparent coating compositions containing a colloidal dispersion of cerium. WO2006072743A2, 2006.

43. Berkei, M.; Nolte, U.; Sawitowski, T. Using CeO_2 for stabilization of organic polymers against free radicals. EP1832624A1, 2007.

44. Kim, S.-K.; Paik, U.; Oh, S.-G.; Park, Y.-K.; Katoh, T.; Park, J.-G. Effects of the Physical Characteristics of Cerium Oxide on Plasma-Enhanced Tetraethylorthosiliate Removal Rate of Chemical Mechanical Polishing for Shallow Trench Isolation. *Jpn. J. Appl. Phys.* **2003,** *42*, 1227-1230.

45. Kockrick, E.; Schrage, C.; Grigas, A.; Geiger, D.; Kaskel, S. Synthesis and catalytic properties of microemulsion-derived cerium oxide nanoparticles. *J. Solid State Chem.* **2008,** *181*, 1614-1620.

46. Brunauer, S.; H., E. P.; Teller, E. Adsorption of Gases in Multimolecular Layers. *J. Am. Chem. Soc.* **1938,** *60*, 309-319.

47. Lindner, P., In *Neutron, X-rays and Light. Scattering Methods Applied to Soft Condensed Matter,* Zemb, T.; Lindner, P., Eds. 2002; pp 23-48.

48. Chane-Ching, J. Y. Cerium (IV) compound readily soluble in water, and method for its preparation. EP208580A1, 1987.

49. Nabavi, M.; Spalla, O.; Cabane, B. Surface Chemistry of Nanometric Ceria Particles in Aqueous Dispersions. *J. Colloid Interface Sci.* **1993,** *160*, 459-471.

50. Kümmerle, E. A.; Heger, G. The Structures of C-$Ce_2O_{3+\delta}$, Ce_7O_{12}, and $Ce_{11}O_{20}$. *J. Solid State Chem.* **1999,** *147*, 485-500.

51. 04-008-6551, S. *ICDD® (International Centre for Diffraction Data)* **2009**.

52. Pedersen, J. S., In *Neutron, X-rays and Light. Scattering Methods Applied to Soft Condensed Matter,* Zemb, T.; Lindner, P., Eds. 2002; pp 391-420.

53. Sehgal, A.; Lalatonne, Y.; Berret, J.-F.; Morvan, M. Precipitation-Redispersion of Cerium Oxide Nanoparticles with Poly(acrylic acid): Toward Stable Dispersions. *Langmuir* **2005,** *21*, 9359-9364.

54. Midmore, B. R. Preparation of a novel silica-stabilized oil/water emulsion. *Coll. Surf. A: Phys. Eng. Asp.* **1998,** *132*, 257-265.

55. Walsh, A.; Thompson, K. L.; Armes, S. P.; York, D. W. Polyamine-Functional Sterically Stabilized Latexes for Covalently Cross-Linkable Colloidosomes. *Langmuir* **2010,** *26*, 18039-18048.

56. Azad, A. R. M.; Ugelstad, J.; Fitch, R. M.; Hansen, F. K. Emulsification and emulsion polymerization of styrene using mixtures of cationic surfactant and long chain fatty alcohols or alkanes as emulsifiers. *ACS Symp. Ser.* **1976,** *24*, 1-23.

57. Choi, Y. T.; El-Aasser, M. S.; Sudol, E. D.; Vanderhoff, J. W. Polymerization of Styrene Miniemulsions. *J. Polym. Sci. Polym. Chem. Ed.* **1985,** *23*, 2973-2987.

58. Blythe, P. J.; Morrison, B. R.; Mathauer, K. A.; Sudol, E. D.; El-Aasser, M. S. Enhanced Droplet Nucleation in Styrene Miniemulsion Polymerization. 1. Effect of Polymer Type in Sodium Lauryl Sulfate/Cetyl Alcohol Miniemulsions. *Macromolecules* **1999,** *32*, 6944-6951.

59. do Amaral, M.; Bogner, A.; Gauthier, C.; Thollet, G.; Jouneau, P.-H.; Cavaillé, J.-Y.; Asua, J. M. Novel Experimental Technique for the Determination of Monomer Droplet Size Distribution in Miniemulsion. *Macromol. Rapid Commun.* **2005,** *26*, 365-368.

60. Xu, H.; Melle, S.; Golemanov, K.; Fuller, G. Shape and Buckling Transitions in Solid-Stabilized Drops. *Langmuir* **2005,** *21*, 10016-10020.

61. Datta, S. S.; Shum, H. C.; Weitz, D. A. Controlled Buckling and Crumpling of Nanoparticle-Coated Droplets. *Langmuir* **2010,** *26*, 18612-18616.

62. Binks, B. P.; Horozov, T. S. Aqueous Foams Stabilized Solely by Silica Nanoparticles. *Angew. Chem. Int. Ed.* **2005,** *44*, 3722-3725.

63. Abkarian, M.; Subramaniam, A. B.; Kim, S.-H.; Larsen, R. J.; Yang, S.-M.; Stone, H. A. Dissolution Arrest and Stability of Particle-Covered Bubbles. *Phys. Rev. Lett.* **2007,** *99*, 188301.

64. Hassander, H.; Johansson, B.; Törnell, B. The mechanism of emulsion stabilization by small silica (Ludox) particles. *Colloids Surfaces* **1989,** *40*, 93-105.

65. Binks, B. P.; Lumsdon, S. O. Stability of oil-in-water emulsions stabilised by silica particles. *Phys. Chem. Chem. Phys.* **1999,** *1*, 3007-3016.

66. Ashby, N. P.; Binks, B. P. Pickering emulsions stabilised by Laponite clay particles. *Phys. Chem. Chem. Phys.* **2000,** *2*, 5640-5646.

67. Binks, B. P.; Lumsdon, S. O. Influence of Particle Wettability on the Type and Stability of Surfactant-Free Emulsions. *Langmuir* **2000,** *16*, 8622-8631.

68. Sheibat-Othman, N.; Bourgeat-Lami, E. Use of Silica Particles for the Formation of Organic-Inorganic Particles by Surfactant-Free Emulsion Polymerization. *Langmuir* **2009,** *25*, 10121-10133.

69. Thieme, J.; Abend, S.; Lagaly, G. Aggregation in Pickering emulsions. *Colloid Polym. Sci.* **1999,** *277*, 257-260.

Table 1: Intensity average diameter, *Poly* value and surface coverage of MMA droplets for various initial CeO_2 amounts.

Expt [a]	CeO_2 (wt%/MMA)	D_d (nm) - *Poly* [b]	Surface coverage (%) [c]
ME 1	0	demixtion	/
ME 2	5	358 – *0.18*	19.1
ME 3	10	236 – *0.16*	25.2
ME 4	15	197 – *0.12*	31.2
ME 5	20	148 – *0.14*	31.4
ME 6	25	139 – *0.17*	36.6
ME 7	30	112 – *0.16*	35.6
ME 8	35	101 – *0.22*	37.3

[a]: All experiments were carried out with MMA: 20wt%/water; ODA: 4 wt%/MMA; [MAA] = 1.85 µmol.m^{-2}; sonication time: 5min. b: Obtained by dynamic light scattering. c: Calculated from equation 2.

Table 2: Summary of experimental conditions of all miniemulsion polymerizations performed in this study

Expt [a]	Monomer(s)	CeO_2 (wt%/MMA)	MAA (µmol.m^{-2})	Time [b] (h)	Conversion (%) [b]	D_d/D_p (nm) [c]	*Poly* [c]	N_d/N_p (L^{-1}_{water})	Cov (%) [e]
						Initial/final [d]			
Latex 1	MMA	20	1.85	0.83	78	148/217	0.14/0.06	$1.4\times10^{17}/3.8\times10^{16}$	31/55
Latex 2	MMA	25	1.85	1	85	139/202	0.17/0.05	$1.8\times10^{17}/4.7\times10^{16}$	37/65
Latex 3	MMA	30	1.85	1.25	83	112/195	0.16/0.09	$3.3\times10^{17}/5.3\times10^{16}$	36/75
Latex 4	MMA	35	1.85	3	85	101/200	0.22/0.05	$4.7\times10^{17}/5.0\times10^{16}$	37/90
Latex 5	MMA	35	1.4	2	86	115/216	0.19/0.02	$3.2\times10^{17}/4.0\times10^{16}$	43/98
Latex 6[f]	MMA	35	1.4	1.5	89	130/249	0.2/0.18	$2.2\times10^{17}/2.6\times10^{16}$	47/111
Latex 7	MMA	25	1.5	1	79	149/203	0.18/0.08	$1.3\times10^{17}/4.4\times10^{16}$	41/68
Latex 8	MMA	25	2.8	1	76	147/248	0.21/0.06	$1.4\times10^{17}/2.5\times10^{16}$	41/82
Latex 9	BA	35	1.4	6	92	190/211	0.26/0.06	$7.3\times10^{16}/4.8\times10^{16}$	67/90
Latex 10[g]	MMA/BA	35	1.4	4.5	96	150/198	0.19/0.09	$1.5\times10^{17}/5.4\times10^{16}$	54/88

[a] All experiments were carried out with monomer(s): 20wt%/water; ODA: 4 wt%/monomer(s); AIBA: 1 wt%/monomer(s) (or $7.5\text{x}10^{-3}$ mol/L_{water}); sonication time: 5min; T=70°C. [b] This time corresponds to the last sample withdrawn before destabilization. [c] Obtained by dynamic light scattering (DLS). [d] "Final" refers to the last sample withdrawn before destabilization. [e] Calculated from equation 2 for the initial coverage using D_d obtained from DLS (as the size of CeO_2 nanoparticles was considered negligible with respect to the size of MMA droplet), and by using modified equation 2 for the final coverage (i.e. D_d is replaced by D_p obtained from DLS, m_M is replaced by m_P the combined amount of MMA and PMMA and ρ_M is replaced by ρ_P the combined density of MMA and PMMA – amounts of unreacted and converted MAA and ODA were neglected, and CeO_2 amount was not taken into account). [f] Isobutyric acid instead of MAA. [g] MMA/BA: 50/50 by weight

Figure 1: a) TEM and b) HRTEM images of the CeO_2 nanoclusters used in this study.

Figure 2: SAXS profiles of a 20 $g.L^{-1}$ dispersion of CeO_2 particles. Experimental data (+). The theoretical scattering curves of the represented structure are plotted using lines (—— corresponds to a monomodal distribution of hard spheres with a diameter of 2.7 nm, whereas – – – fits with the form factor of a cluster composed of 7 spheres of 2.7 nm each).

Figure 3: Evolution of the droplet diameter (D_d, ◆) and of the sample dispersity (*Poly*, ◆) versus MAA concentration for MMA miniemulsions stabilized by 25 wt% of CeO_2 with respect to MMA (MMA: 20 wt%/water; ODA: 4 wt%/MMA).

Figure 4: Evolution of the droplet diameter (D_d, ◆) and surface coverage (●) *versus* the amount of CeO_2 for MMA miniemulsions. MMA: 20 wt%/water; ODA: 4 wt%/MMA; [MAA] = 1.85 $\mu mol.m^{-2}$.

Figure 5: TEM images of MMA droplets prepared in the presence of 35 wt% CeO_2 (ME8 sample, Table 1): a) dry specimen; b,c) ice-embedded droplets from the quench-frozen suspension immediately after the preparation of the miniemulsion. The arrows in b point to droplets with a very low contrast; d) ice-embedded droplets from the same suspension after one week of ageing.

Figure 6: Evolution of a) conversion versus time, b) particle diameter versus time, c) particle number versus conversion and d) surface coverage versus conversion for MMA miniemulsion

polymerization using various initial amounts of CeO_2 (wt%/MMA). All experiments were carried out with MMA: 20 wt%/water; ODA: 4 wt%/MMA; AIBA: 1 wt%/MMA; [MAA] = 1.85 µmol.m^{-2}; T = 70°C.

Figure 7: TEM images of Latex 4 (35 wt% CeO_2): a,b) quench-frozen suspension; c) dry preparation at low temperature; d) ultrathin section of epoxy-embedded Latex 2 (25 wt% CeO_2 – *Conversion* = 80%, sample taken just before destabilization) – MMA: 20 wt%/water; ODA: 4 wt%/MMA; AIBA: 1 wt%/MMA; [MAA] = 1.85 µmol.m^{-2}; T = 70°C.

Figure 8: Evolution of a) conversion versus time and b) diameter versus conversion for the miniemulsion polymerization of MMA (Latex 5), BA (Latex 9) or MMA/BA 50/50 wt% (Latex 10). All experiments were carried out with 20 wt% of monomer(s)/water; CeO_2: 35 wt%/monomer(s); ODA: 4 wt%/monomer(s); AIBA: 1 wt%/ monomer(s); [MAA] = 1.4 µmol.m^{-2}; T = 70°C.

Figure 9: Cryo-TEM images of Latex 9 (35 wt% CeO_2; BA: 20 wt%/water; ODA: 4 wt%/BA; AIBA: 1 wt%/BA; [MAA] = 1.4 µmol.m^{-2}; T = 70°C). The arrows in a) point to "assemblies" of CeO_2 nanoclusters with an ill-defined interface, those in b) to nanoceria detached from their parent particles.

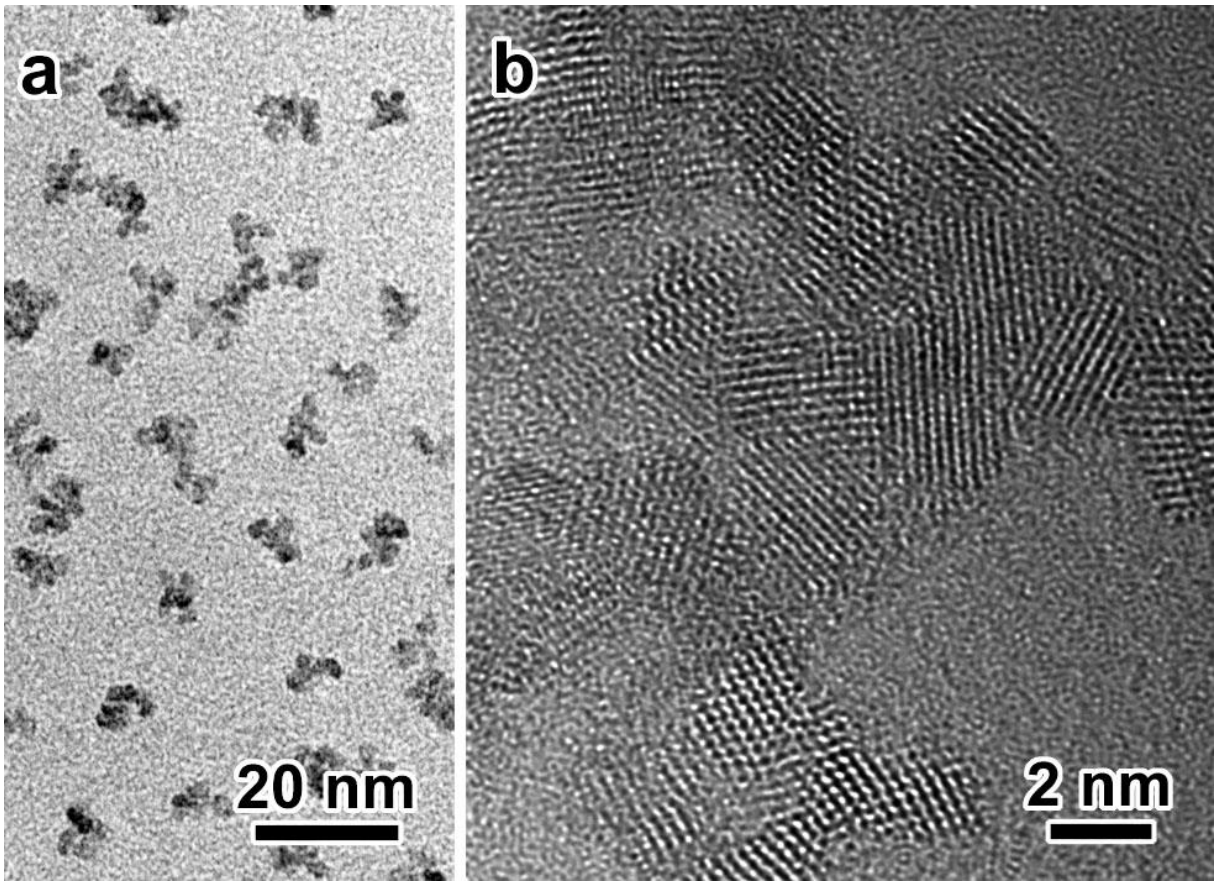

Figure 1: a) TEM and b) HRTEM images of the CeO_2 nanoclusters used in this study.

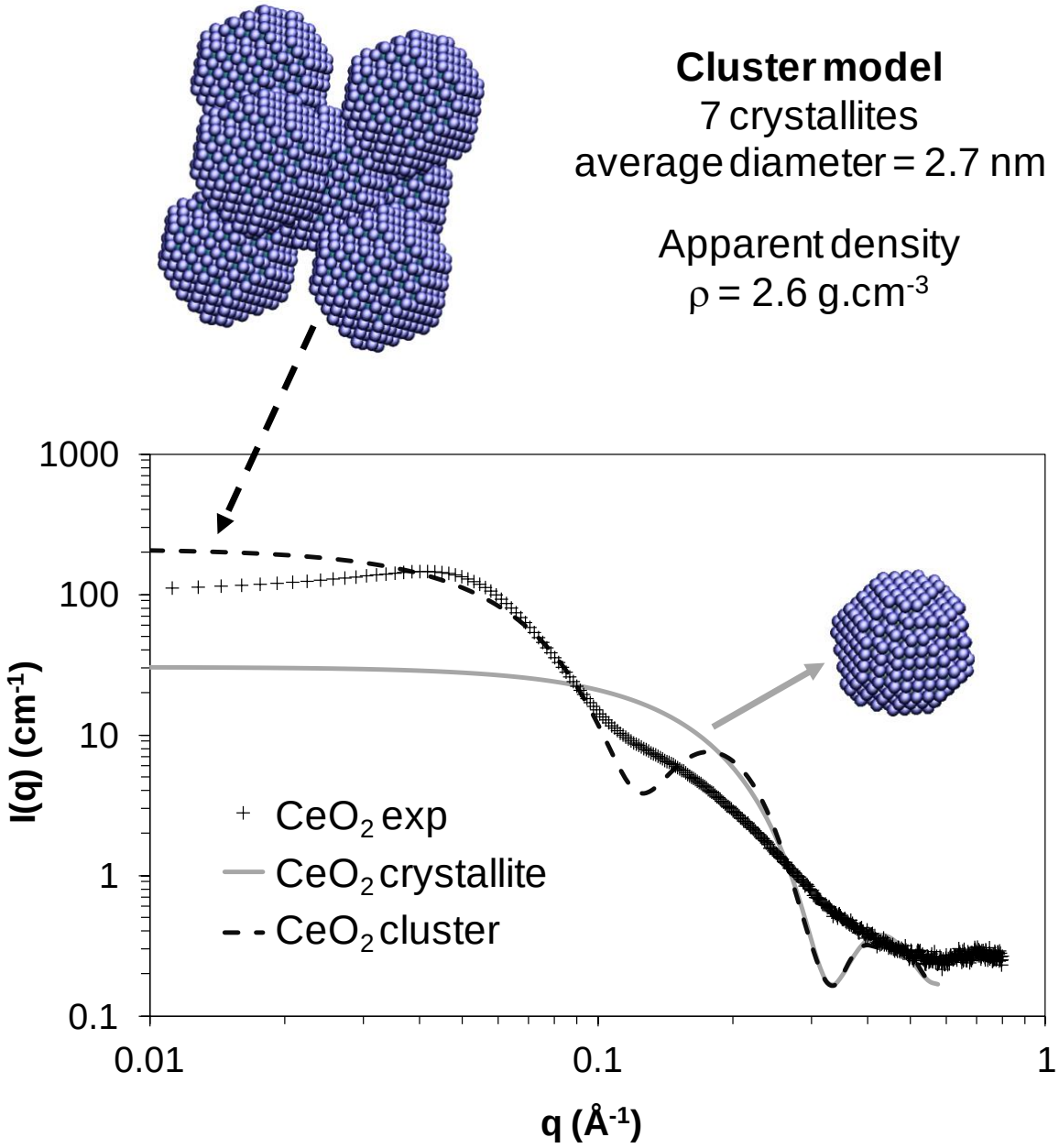

Figure 2: SAXS profiles of a 20 g.L^{-1} dispersion of CeO_2 particles. Experimental data (+). The theoretical scattering curves of the represented structure are plotted using lines (—— corresponds to a monomodal distribution of hard spheres with a diameter of 2.7 nm, whereas – – – fits with the form factor of a cluster composed of 7 spheres of 2.7 nm each).

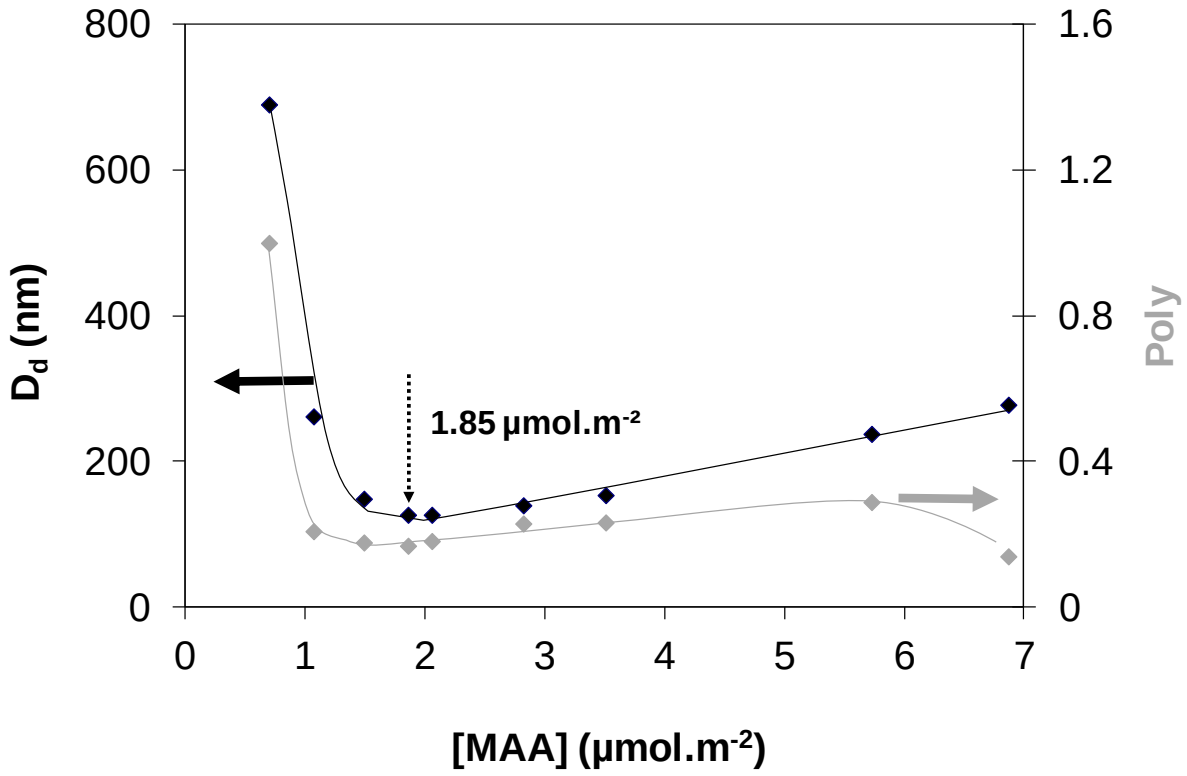

Figure 3: Evolution of the droplet diameter (D_d, ◆) and of the sample dispersity (*Poly*, ◆) versus MAA concentration for MMA miniemulsions stabilized by 25 wt% of CeO_2 with respect to MMA (MMA: 20 wt%/water; ODA: 4 wt%/MMA).

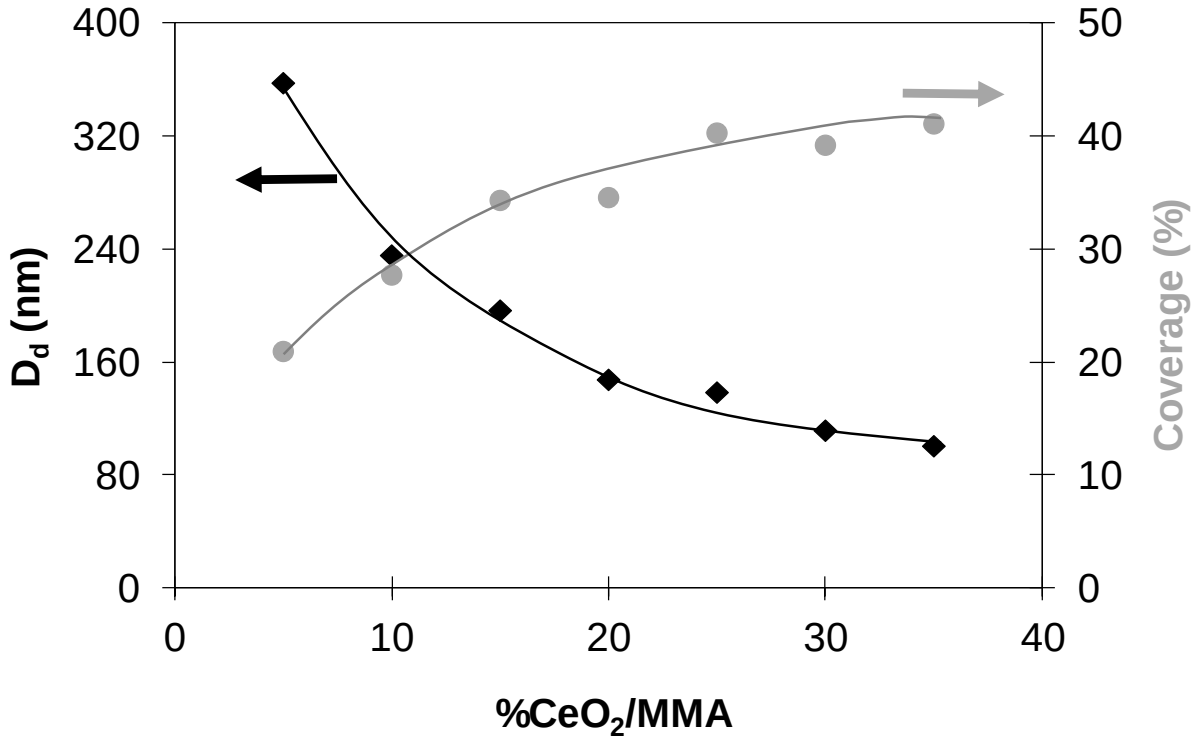

Figure 4: Evolution of the droplet diameter (D_d, ◆) and surface coverage (●) *versus* the amount of CeO_2 for MMA miniemulsions. MMA: 20 wt%/water; ODA: 4 wt%/MMA; [MAA] = 1.85 µmol.m^{-2}.

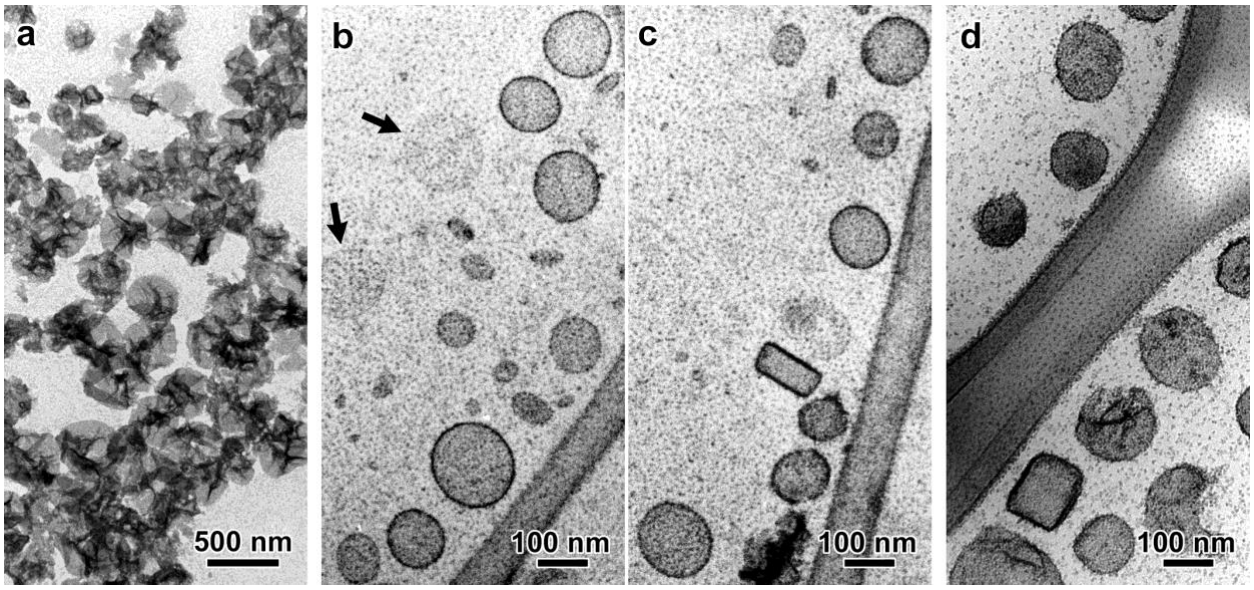

Figure 5: TEM images of MMA droplets prepared in the presence of 35 wt% CeO_2 (ME8 sample, Table 1): a) dry specimen; b,c) ice-embedded droplets from the quench-frozen suspension immediately after the preparation of the miniemulsion. The arrows in b point to droplets with a very low contrast; d) ice-embedded droplets from the same suspension after one week of ageing.

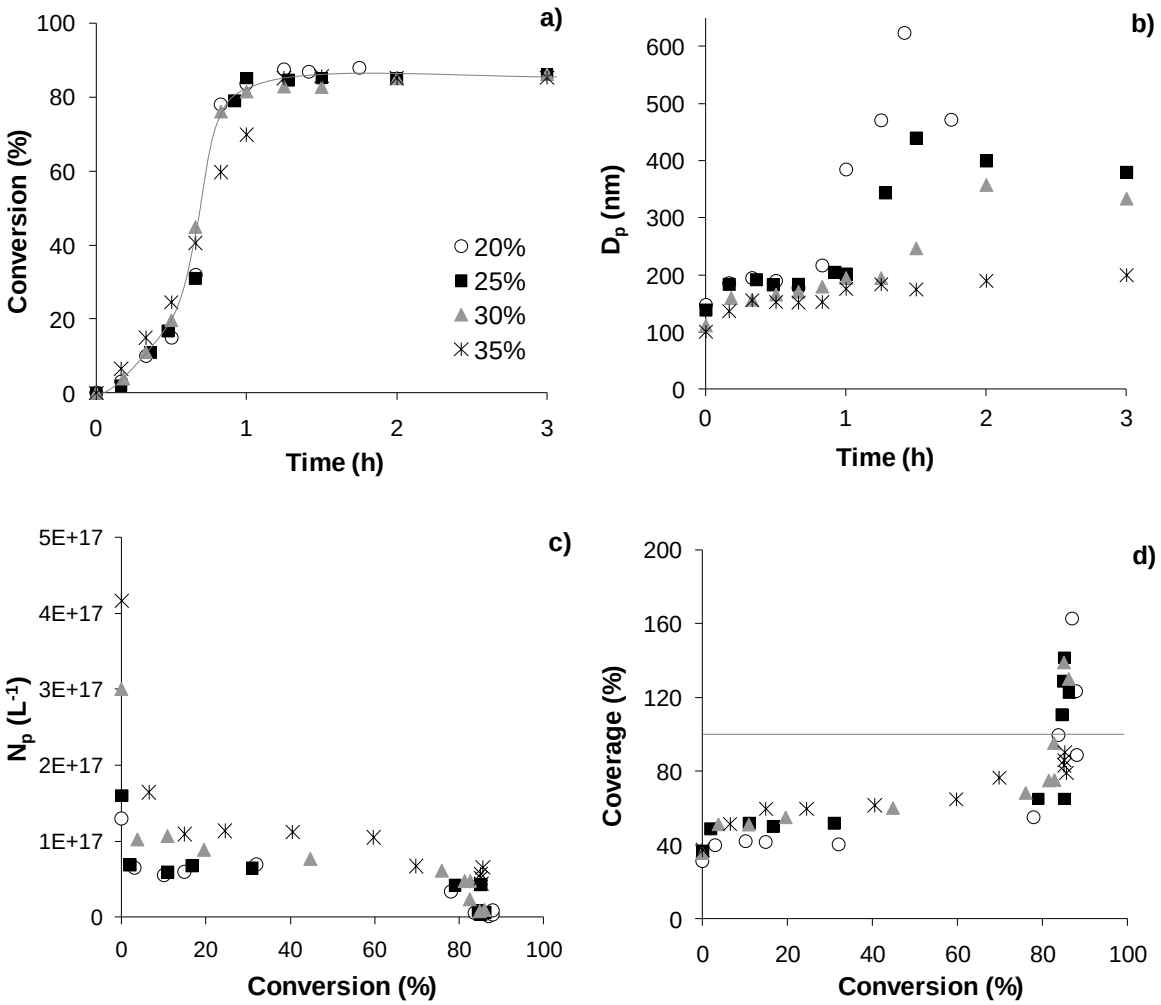

Figure 6: Evolution of a) conversion versus time, b) particle diameter versus time, c) particle number versus conversion and d) surface coverage versus conversion for MMA miniemulsion polymerization using various initial amounts of CeO_2 (wt%/MMA). All experiments were carried out with MMA: 20 wt%/water; ODA: 4 wt%/MMA; AIBA: 1 wt%/MMA; [MAA] = 1.85 µmol.m^{-2}; T = 70°C.

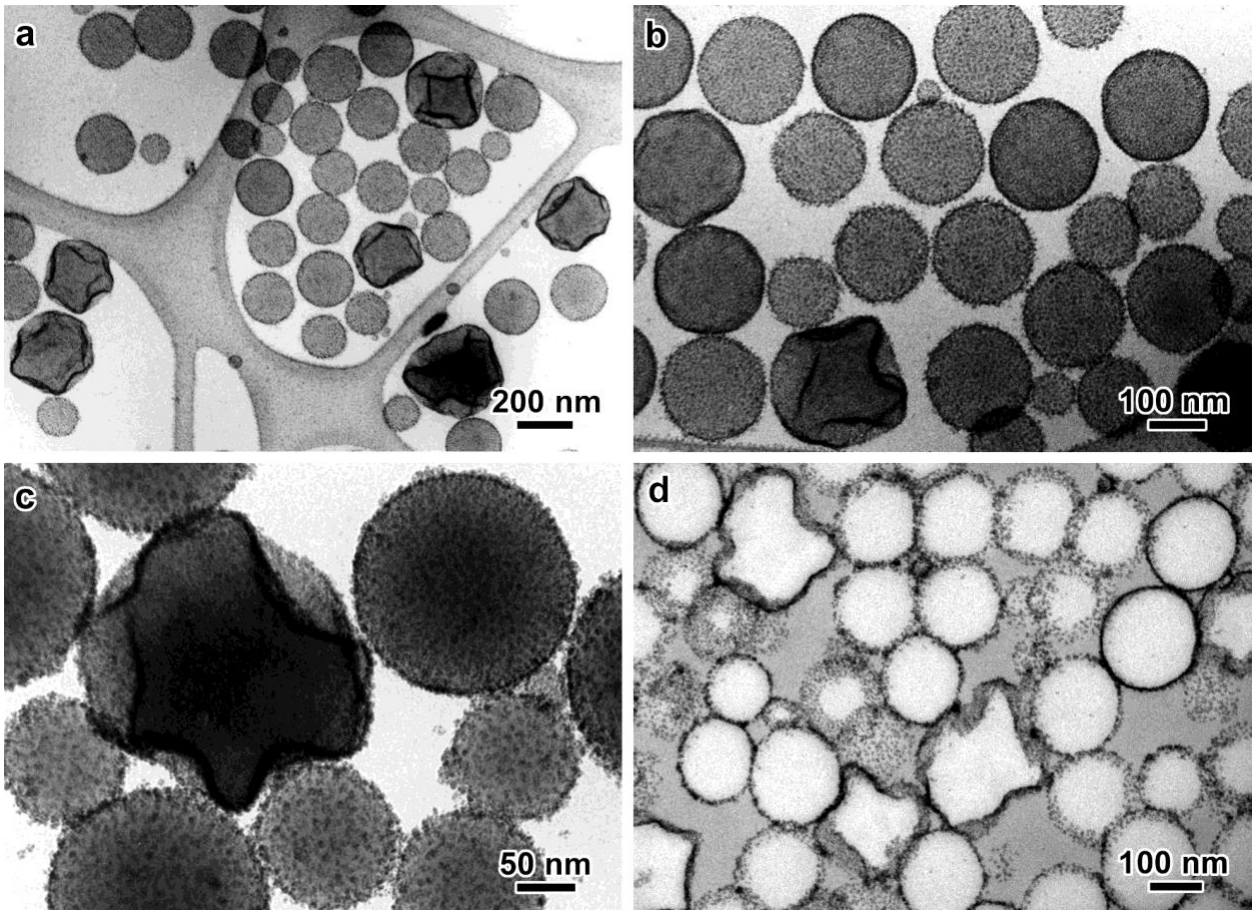

Figure 7: TEM images of Latex 4 (35 wt% CeO_2): a,b) quench-frozen suspension; c) dry preparation at low temperature; d) ultrathin section of epoxy-embedded Latex 2 (25 wt% CeO_2 – *Conversion* = 80%, sample taken just before destabilization) – MMA: 20 wt%/water; ODA: 4 wt%/MMA; AIBA: 1 wt%/MMA; [MAA] = 1.85 µmol.m^{-2}; T = 70°C.

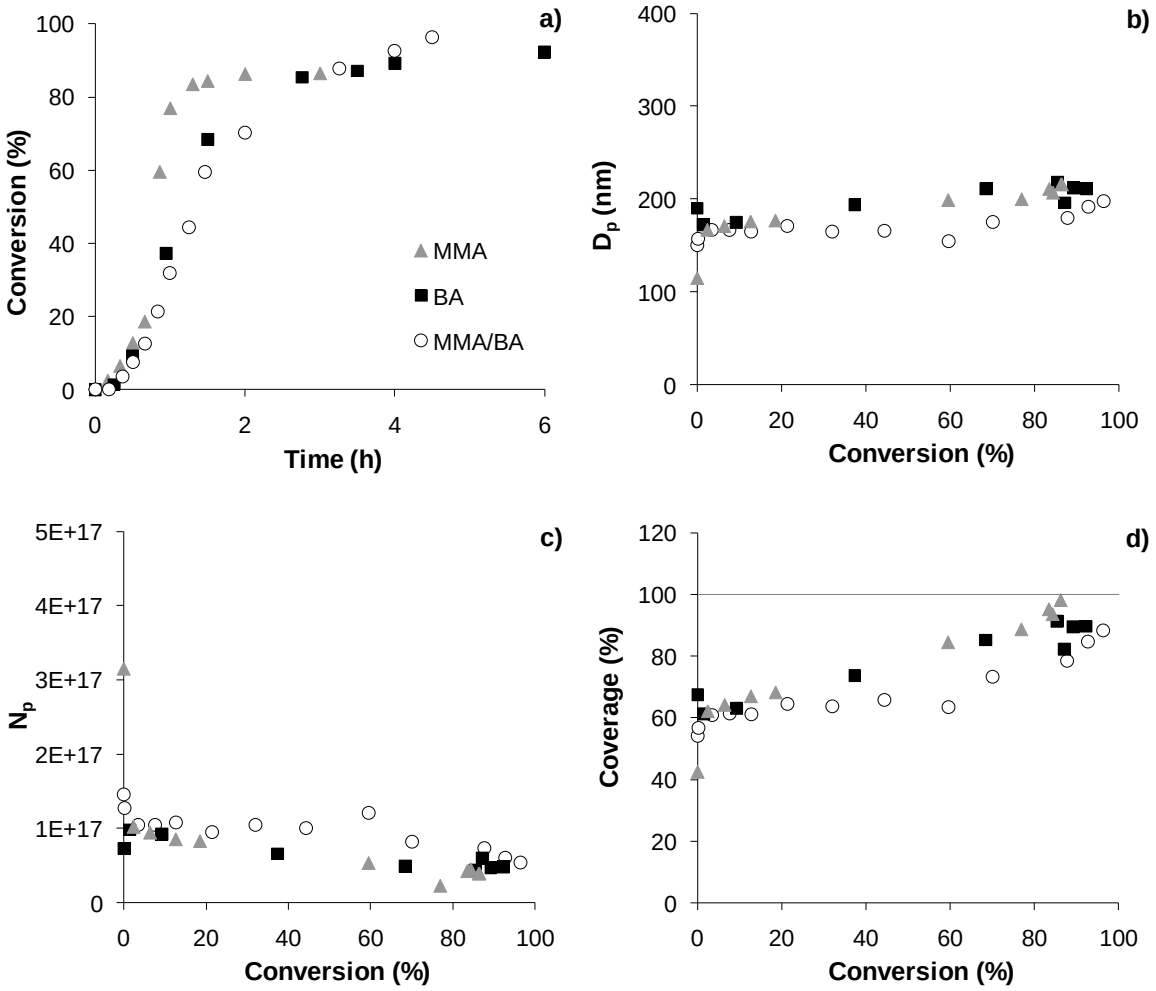

Figure 8: Evolution of a) conversion versus time and b) diameter versus conversion for the miniemulsion polymerization of MMA (Latex 5), BA (Latex 9) or MMA/BA 50/50 wt% (Latex 10). All experiments were carried out with 20 wt% of monomer(s)/water; CeO_2: 35 wt%/monomer(s); ODA: 4 wt%/monomer(s); AIBA: 1 wt%/ monomer(s); [MAA] = 1.4 µmol.m^{-2}; T = 70°C.

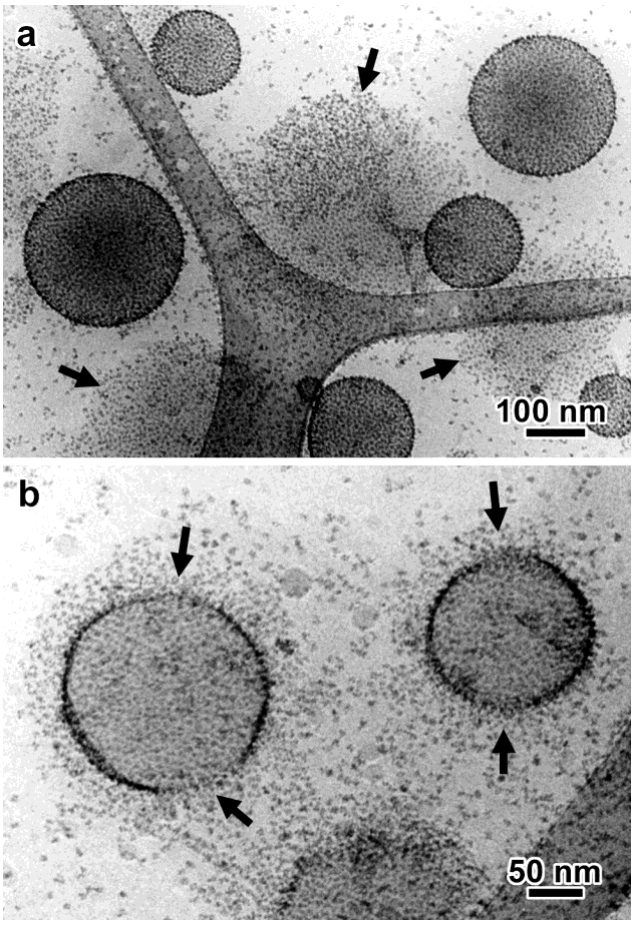

Figure 9: Cryo-TEM images of Latex 9 (35 wt% CeO_2; BA: 20 wt%/water; ODA: 4 wt%/BA; AIBA: 1 wt%/BA; [MAA] = 1.4 µmol.m^{-2}; T = 70°C). The arrows in a) point to "assemblies" of CeO_2 nanoclusters with an ill-defined interface, those in b) to nanoceria detached from their parent particles.

For Table of Contents only